Bone Reports 21 (2024) 101763

Contents lists available at ScienceDirect

Bone Reports

journal homepage: www.elsevier.com/locate/bonr

Chloride/proton antiporters ClC3 and ClC5 support bone formation in mice

Irina L. Tourkova [a,b,1], Quitterie C. Larrouture [a,1], Silvia Liu [a], Jianhua Luo [a], Katherine E. Shipman [c], Kelechi M. Onwuka [a], Ora A. Weisz [c], Vladimir Riazanski [d], Deborah J. Nelson [d], Matthew L. MacDonald [e], Paul H. Schlesinger [f], Harry C. Blair [a,b,*]

[a] Department of Pathology, University of Pittsburgh, Pittsburgh, PA, USA
[b] Research Service, VA Healthcare System, Pittsburgh, PA, USA
[c] Renal Electrolyte Division, Department of Medicine, University of Pittsburgh School of Medicine, Pittsburgh, PA, USA
[d] Dept of Neurobiology, Pharmacology & Physiology, University of Chicago, Chicago, IL, USA
[e] Department of Psychiatry, University of Pittsburgh School of Medicine, Pittsburgh, PA, USA
[f] Department of Cell Biology, Washington University, St. Louis, MO, USA

ARTICLE INFO

Keywords:
ClC3
ClC5
Bone formation rate
Mineral transport

ABSTRACT

Acid transport is required for bone synthesis by osteoblasts. The osteoblast basolateral surface extrudes acid by Na^+/H^+ exchange, but apical proton uptake is undefined. We found high expression of the Cl^-/H^+ exchanger ClC3 at the bone apical surface. In mammals ClC3 functions in intracellular vesicular chloride transport, but when we found Cl^- dependency of H^+ transport in osteoblast membranes, we queried whether ClC3 Cl^-/H^+ exchange functions in bone formation. We used ClC3 knockout animals, and closely-related ClC5 knockout animals: *In vitro* studies suggested that both ClC3 and ClC5 might support bone formation. Genotypes were confirmed by total exon sequences. Expression of ClC3, and to a lesser extent of ClC5, at osteoblast apical membranes was demonstrated by fluorescent antibody labeling and electron microscopy with nanometer gold labeling. Animals with ClC3 or ClC5 knockouts were viable. In ClC3 or ClC5 knockouts, bone formation decreased ~40 % by calcein and xylenol orange labeling *in vivo*. In very sensitive micro-computed tomography, ClC5 knockout reduced bone relative to wild type, consistent with effects of ClC3 knockout, but varied with specific histological parameters. Regrettably, ClC5-ClC3 double knockouts are not viable, suggesting that ClC3 or ClC5 activity are essential to life. We conclude that ClC3 has a direct role in bone formation with overlapping but probably slightly smaller effects of ClC5. The mechanism in mineral formation might include ClC H^+ uptake, in contrast to ClC3 and ClC5 function in cell vesicles or other organs.

1. Introduction

Osteoblasts form an epithelial-like layer separating the extracellular fluid (ECF) from bone (Blair et al., 2023). These cells express specific mechanisms for matrix and mineral formation, including transport of phosphate to produce bone mineral, hydroxyapatite. Transport protein expression declines with age, as reported recently (Tourkova et al., 2023). The production of hydroxyapatite from calcium, phosphate, and hydroxide, evolves a massive acid flux. Thus, removal of acid is essential to mineralization. Previously we showed high expression of Na/H exchanger 1 (NHE1) at the secretory osteoblast basolateral surfaces neutralize massive acid loads (Liu et al., 2011), modified by the sodium-hydrogen exchange regulatory protein NHERF (Liu et al., 2012).

We hypothesized on this basis that high-capacity proton transport from matrix into osteoblast cytosol must exist to support acid transport (Schlesinger et al., 2020). Gene screening in mineralizing osteoblasts had shown dramatic expression of chloride-proton antiporter ClC3. Other related proteins, particularly ClC5, are highly expressed (Blair et al., 2018). *In vitro,* ClC3 and ClC5 double negative osteoblasts do not mineralize (Larrouture et al., 2015). The transporter ClC3 has been studied carefully as an intracellular membrane protein involved in vesicular chloride transport for secretion in endosomes and synaptic vesicles with specific targeting mechanisms (Salazar et al., 2004; Stauber et al., 2012). Expression of ClC3 in high concentrations at other sites is not consistent with this role. On the other hand, using isolated osteoblast membrane vesicles made by nitrogen cavitation, we showed chloride

* Corresponding author at: 705 Scaife Hall, University of Pittsburgh, Pittsburgh, PA 15261, USA.
E-mail address: hcblair@pitt.edu (H.C. Blair).
[1] Contributed equally to this work.

https://doi.org/10.1016/j.bonr.2024.101763
Received 9 April 2024; Accepted 12 April 2024
Available online 16 April 2024

dependent H^+ uptake, which suggested direct H^+/Cl^- exchange (Blair et al., 2018). The biology is complex, and among unresolved issues, in addition to targeting mechanisms (Salazar et al., 2004) is the degree to which heterodimers (Stauber et al., 2012) or other complexes of ClCs may be active in physiology.

We studied the role of ClC3 and the closely related ClC5 in bone mineralization *in vivo* using knockout mice. The ClC3 functional knockout was made by recombination to produce a gene missing a critical exon (Dickerson et al., 2002). The ClC5 knockout, made recently using Crispr-Cas9 recombination, produces no ClC5 (Shipman et al., 2023). We studied distribution of ClCs in osteoblasts, and compared wild type and knockout animals for physical characteristics including mineralization rate in bone and detailed morphometry by micro-computed tomography. We find that ClC3 or ClC5 knockouts reduce bone formation, with some variation of effects. Changes in dentition and renal function also occurred in CLC5 knockouts, in keeping with other studies of ClC5 defects. Regrettably, ClC3-ClC5 double knockouts are not viable, so the interaction of ClC3 and ClC5 in bone will require further study.

2. Materials and methods

2.1. Animals

Animal protocols were approved by University of Pittsburgh Institutional Animal Care and Use Committee. The same number of male and female mice were used in each age category; male and female animals in specific experiments are indicated. Mice were 4–6 months of age unless specified. C57BL/6J mice were from the Jackson Laboratory (Bar Harbor, ME, USA).

2.2. ClC3 knockout mice

Mice lacking functional ClC3 were the kind gift of Fred S Lamb, Vanderbilt University. These animals have a targeted deletion of the last part of exon 6 and all of exon 7 containing transmembrane domains 3 and 4, with a cassette containing neomycin resistance (Dickerson et al., 2002) in hybrid 129/Sv and C57BL/6J mice. These mice were inbred seven generations into C57BL/6J for a uniform background. Breeding into C57BL/6J was followed by automated genotyping by Transnetyx (Cordova, TN, USA) proprietary TaqMan assays to identify the knockout (Dickerson et al., 2002) and full length wild-type transcript. We verified the ClC3 knockout mice after C57BL/6 inbreeding by whole exome sequencing (Supplemental Fig. 1).

2.3. ClC5 knockout mice

These mice were recently produced (Shipman et al., 2023). Briefly, 129-Elite Mouse 129S2/SvPasCrl (Charles River) zygotes, by *in vitro* fertilization, were injected with a mixture of EnGen Cas9 protein (New England Biolabs), Clcn5-E211-guide3 sgRNA and Clcn5-E211X-HDR ss-ODN (Shipman et al., 2023) designed using MIT's guide sequence generator. Embryos were transferred to pseudopregnant CD1 recipients. Tail genomic DNA for the CRISPR edited pups were tested by PCR and sequencing. A founder male carrying a 189 bp deletion was chosen that included half of exon 6 and the intron junction, preventing splicing of intron 6, resulting in knockout of ClC5. It was backcrossed to WT C57BL/6J three generations.

2.4. Whole exome sequencing

Livers were obtained from 5 month old male WT, ClC3 knockout and ClC5 knockout mice. Samples were sequenced on an illumina HiSeq2500 (Illumina Inc., CA). Structures of knockout genes were verified by whole exome sequencing at the University of Pittsburgh Sequencing Center; key regions sequenced are shown in Supplemental Fig. 1. Homologous regions of ClCs were examined and showed no deletions.

2.5. Differentiation of osteoblasts in vitro

In addition to assays of WT and knockout animals, we isolated stromal stem cells (Larrouture et al., 2021) and differentiated osteoblasts on perforated polyethyene terphthalate (PET) membranes (Larrouture et al., 2021). This method is reproducible and produces dense and uniform osteoblasts of wild type and knockout strains. Analysis by micro CT and labeling of bone with calcein and xylenol orange were as described (Robinson et al., 2023).

2.6. Histomorphometry

Lumbar vertebrae 1–3 were used for dynamic histomorphometry and histology; lumbar vertebrae 4–5 were used for micro-computed tomography (μCT) as described (Robinson et al., 2023). Briefly, lumbar vertebrae were fixed overnight in 3.7 % formalin, then transferred to 70 % ethanol for μCT using a Bruker Skyscan 1172 using a bone density cutoff of 150 mg/cm^2, at 6 μm resolution. Scans were analyzed using Bruker CTan software for trabecular parameters; three-dimensional images were produced with Bruker CTvox software. For dynamic histomorphometry vertebral sections used animals labeled with xylenol orange and calcein (Robinson et al., 2023). Animals were labeled with 20 μg/g mouse weight of calcein 5 days prior sacrifice and 80 μg/g mouse weight with xylenol orange 2 days prior to sacrifice. A minimum of four sections per animal cut at 6 μm were used and were analyzed blindly relative to genotype, with results categorized by genotype after analysis. This proved difficult: initial analysis failed to distinguish groups consistently despite μCT data showing clear differences (*cf.* Fig. 5). Therefore, this work was repeated, formally blinded, with vertebrae photographed as 420 μm fields in red and green fluorescence and overlain with phase to show bone trabeculae, a minimum of four sections per genotype, using areas subjacent to growth plates of vertebrae to avoid artifacts from cortical bone or growth plates (*cf.* Fig. 3A-C).

2.7. RNA isolation and real-time PCR

Total RNA was isolated by oligo dT affinity (RNeasy; Qiagen, Valencia, CA), and reverse transcribed with random hexamers and reverse transcriptase (Superscript III, Invitrogen, Thermo-Fisher). PCR was performed using an Applied Biosystems StepOne Plus instrument (Life Technologies) in 10 μl reaction mixtures with fast SYBR green master mix (Applied Biosystems), 250 nM primers and cDNA. Expression relative to mouse β-actin or glyceraldehyde-3-phosphate dehydrogenase cDNA was calculated (Tourkova et al., 2017). PCR used 95 °C denaturation 30 s, 58 °C annealing 30 s, and 72 °C elongation 1 min, 32 cycles. Triplicate assays, each run in duplicate, were performed. Product sizes were verified by electrophoresis on 2 % agarose. For primers, see Methods.

2.8. Stromal stem cell (SSC) isolation and differentiation

SSCs were from C57Bl/6 J mouse femoral or tibial bone marrow as described (Tourkova et al., 2023), of wild type or knockout animals. Cell characteristics were verified by flow cytometry showing essentially uniform expression of CD44 and Sca1, but not of CD45 (negative control) using a FACScalibur instrument (Becton Dickinson, San Diego, CA) with analysis by Cell Quest Software (Becton Dickinson). Briefly, cell pellets were incubated 20 min with antibodies conjugated with fluorescein isothiocyanate (FITC). Isotype matched mouse antibodies conjugated with FITC were negative controls for background. SSC were grown in proliferation medium, Dulbecco's Modified Essential Medium (DMEM) with1 g/l glucose, 10 % FBS and antibiotic-antimycotics. For osteogenic differentiation medium was supplemented with 10 mM 2-

phosphoglycerol, 30μg/ml ascorbic acid, and 0.5 mM $CaCl_2$ (final Ca^{2+} 2 mM). Cells were grown on polyethylene terephthalate membranes, 12 μm thick with 2 × 10^6 0.4 μm perforations/cm^2, 4.2 cm^2 surface (Transwells, Falcon, Corning NY). This method produces consistent uniform osteoblast differentiation (Larrouture et al., 2021).

2.9. Fluorescent antibody assays

Cell culture on Transwells were fixed on day 14 with 3.7 % formaldehyde for 10 min followed by permeabilization with 0.1 % Triton X-100 for 20 min. After blocking with 2 % BSA, the cells were incubated with primary antibody against C-terminal regions of ClC3 or ClC5 (Alomone Labs, Israel) at 1:100 at 4 °C overnight and then with Alexa Fluor 488- or 555- conjugated secondary antibodies (Life Technologies) (green or red, respectively) at room temperature for 1 h, except for fluorescent labeling of ClC3 in mouse bone of wild type or ClC3 knockout animals which used rabbit polyclonal anti-ClC3 raised to amino acids 80–125 of human ClC3 (Bioss, Woburn, MA), 1:400 followed by fluorescent secondary antibodies as above. Following this 4′,6-diamidino-2-phenylindole (DAPI) was applied for 5 min to label nuclei. Cell cultures on transwells were mounted on slides in Fluoroshield (Abcam, Cambridge, UK). Additionally, tartrate resistant acid phosphatase was labeled in sections of wild-type and ClC3 or ClC5 knockout animals using rabbit polyclonal antibody reactive to mouse (and human) PA5-116970 raised to Rabbit TRAP antigen. Bound antibody was visualized with red-fluorescent secondary label, with controls having no primary antibody. Briefly, sections were de-parrafinized, heated to 64 °C overnight, blocked in 1 % albumin in PBS, incubated with primary antibody 1:100 at room temperature overnight, and then with secondary antibody at 1:1000 for two hours. Between steps, sections were rinsed three times with PBS buffer. For all antibody labeling, Images were acquired on a Nikon TE2000 inverted fluorescence microscope using a 12-bit 1600 × 1200-pixel charge-coupled device.

2.10. Alkaline phosphatase activity, collagen and mineralization

Alkaline phosphatase activity was determined in citrate-buffered saline at pH 8.0 using 0.01 % naphthol phosphate with 0.25 mg/ml fast blue to precipitate the alkaline phosphatase product, an insoluble blue adduct. Sirius red and fast green staining were used to distinguish collagen from non-collagenous proteins (Chondrex, Woodinville WA). Mineralization was evaluated by silver nitrate (Von Kossa) stain. Cells were rinsed with H_2O and fixed with 3.7 % formalin for 2 min. Then, cultures were incubated with 2 % $AgNO_3$ under UV light 10 min and washed.

2.11. Assays for alkaline phosphatase and TRAP in serum

Serum was prepared from intra-cardiac blood of mice at sacrifice. After 45 min at 20 °C and 10 min centrifugation at 200 ×*g*, serum tartrate-resistant acid phosphatase and alkaline phosphatase (ALP) proteins were determined in WT, ClC3 knockout and ClC5 knockout mice using ELISAs (Biomatik USA, Wilmington, Delaware). Serum analysis used a minimum of 4 animals per group.

2.12. Antibody gold-labeled transmission EM

This used cells on Transwell inserts (Larrouture et al., 2021) or vertebral sections from mice. Samples were post-fixed in 1 % OsO_4 with 1 % $K_3[Fe(CN)_6]$, dehydrated in ethanol and embedded. Thin sections (65 nm) were stained with uranyl acetate and lead citrate. Antibody labeling used carbon-coated nickel grids blocked 1 h in BSA, then primary antibody 1 h, washed, then secondary antibody 1 h, washed, and counterstained with 2 % uranyl acetate for 10 min. Primary antibodies were 1:100 for ClC3 and ClC5 (Alomone Labs) or ALP (R&D Systems). Secondary antibody was colloidal gold–conjugated donkey anti-rabbit IgG at 1:20 (Jackson ImmunoResearch). Isotype controls were rabbit and goat sera (Jackson ImmunoResearch). Samples were imaged on a JEOL 1400 Plus with an AMT 2000 pixel square digital camera (Advanced Microscopy Techniques, Danvers, MA).

2.13. Proteomics of ClC3 and ClC5 expression

Analysis used liver or stromal stem cells differentiated to form osteoblasts, from wild type, ClCN3, and ClCN5 knockout animals by mass spectrometry (Puig et al., 2023). Briefly, tandem mass tag labeled peptides on a PepMap RSLC C18 column were eluted by gradients. Sample eluate was electrosprayed into an Orbitrap Eclipse Mass Spectrometer (ThermoFisher Scientific) for analysis. Spectrometry files were processed in Proteome Discoverer v. 2.5 (ThermoFisher Scientific). MS spectra were searched against the *Mus musculus* SwissProt database (http://www.ebi.ac.uk/swissprot). Proteins of high confidence were retained for analyses and protein values were log2 transformed prior to analysis to detect differentially expressed (DE) proteins in the knockout and wild type.

2.14. Protein structures

Structure of ClC3 and the functional ClC3 knockout were calculated from sequences as pdb (Protein Data Bank) files using IntFOLD7 (McGuffin et al., 2023). From these structures, mages were produced using the pdb imaging program https://www.rcsb.org/3d-view with the region knocked out indicated (see Supplemental Fig. 2A-B). These structures were studied further using Visual Molecular Dynamics software, University of Illinois http://www.ks.uiuc.edu/Research/vmd/ for the alignment of the canonical and mutated ClC3 sequences with minimal root mean square differences (see Supplemental Fig. 2C).

2.15. Statistics

Analysis used Prism 10 (GraphPad, California, USA). Comparisons used one-way ANOVA with Dunnett Multiple comparison, or Student's unpaired *t*-test. Significance was concluded at $p < 0.05$. Individual results and standard deviation are shown. Where males and females are identified by color only some comparisons, where there was no significant difference with sex. For brevity, exact *p*-values are shown in figures, and repeated in text only as necessary.

3. Results

3.1. ClC3 and ClC5 knockout animals

Whole exome sequencing of both knockouts was done. The deletion in the ClCN3 functional knockout is shown (Fig. 1A); it previously was characterized by PCR and Southern analysis (Dickerson et al., 2002). The result of the ClC5 knockout is complete absence of protein (Fig. 1B). In ClC5 Crispr-Cas9 deletion causes chain termination and no mature protein is produced (Shipman et al., 2023). Sequencing stack-up comparisons are also shown, (Supplemental Fig. 1; full sequences: https://www.ncbi.nlm.nih.gov/bioproject/PRJNA1064390. We compared abundance of a unique peptide in the wild type and ClC3 knockout in osteoblasts from stromal stem cells by mass spectrometry. Mass spectroscopy proteomics expression data showed confirmed that ClC3 knockout expresses less of the dysfunctional protein than the control: ~40 % reduction of quantity (Fig. 1C). The ClC5 knockout expressed no CLC5, verified by PCR (Fig. 1B).

Since the development of the ClC3 knockout, it became practical to calculate the structure of the membrane proteins. This was done for ClC3 and the knockout using IntFOLD7 (McGuffin et al., 2023). This confirms elimination in the ClC3 knockout of critical transmembrane sequences of the protein, resulting in major structural changes (Supplemental Fig. 2A-B). The knockout is adjacent to the critical E224 for coupling that

maintains anion gating (Rohrbough et al., 2018). These structures were also used in the alignment of the canonical and mutated ClC3 sequences (Supplemental Fig. 2C), which confirmed the maintenance of the structure after the deletion site, in keeping with the maintenance of most of the knockout protein rather than its complete degradation (Fig. 1C), which is typical of denatured proteins.

Viability of the ClC3 knockout was ~50 % at six months, as reported for males or females (Shipman et al., 2023). Viability of the ClC5 knockout was reduced by a similar amount, but it was not practical to quantify because effects on other organs required sacrifice of affected animals (Supplemental Fig. 3).

3.2. Labeling ClC3 and ClC5 at the matrix surface in murine bone by fluorescent antibody microscopy and by antibody gold labeling in transmission electron microscopy

In other reports, ClC3 function has been studied in intracellular vesicles (Stauber et al., 2012); surface expression of ClC3 and ClC5 is controversial. At the light microscopic level, antibodies to ClC3 and ClC5 suggested that these proteins occur at the surface of osteoblasts in trabeculae. Trabecular structure is shown in Fig. 2A, and labeling of the trabecular bone surface for ClC3 or ClC5 in Fig. 2B-C. Concern that this reflects artifact was addressed using an antibody to ClC3 that recognizes the deleted region of ClC3 (Larrouture et al., 2015). This did not show bone labeling in the ClC3 knockout (Fig. 2D). Antibodies to the C-terminal region (Alomone Labs) detected ClC3 in knockout and control bone; anti-actin controls were not affected (not illustrated). Note that human and mouse ClC3 antibodies are cross reactive; the proteins differ only in two conservative amino acid substitutions.

It is not possible to show cell membrane labeling at the light level. We studied labeling in transmission EM with gold-labeled antibodies to ClC3 and ClC5. The ClCs were found at apical secretory surfaces facing the bone matrix (Fig. 2E-F).

3.3. Effect of ClC3 or ClC5 knockouts on bone formation

A key issue is whether presence of ClC3 or ClC5 affects dynamic bone formation (Fig. 3). Examples of fluorescent labels in each genotype in high-resolution images are also shown, overlain on phase to show the trabecular structure (Fig. 3A-C). In detailed blinded quantitative analysis of high-resolution images, we compared male and female animals (males indicated by blue dots; females by red dots, Fig. 3D-E). Minor differences in labeled area of trabecular bone relative to total area, or with sex, occurred (Fig. 3D). On the other hand, the rate of mineral apposition is reduced by ~40 % in the ClC3 or ClC5 knockout mice relative to the wild type control in animals at 4–6 months of age, with these changes significant relative to wild type but not between the ClC3 and ClC5 knockout animals (Fig. 3E). In keeping with the quantitative analysis, by direct imaging interlabel distance appeared relatively narrow in the ClC3 or ClC5 knockout (Fig. 3B-C) relative to the wild type (Fig. 3A). This was followed by blinded measurements of bone parameters by micro-computed tomography (*cf.* Fig. 5, below).

3.4. Weights of animals and serum markers of bone formation and resorption

Animal weights at 5 months and serum alkaline phosphatase (a bone formation marker) and tartrate-resistant acid phosphatase (a bone resorption marker) were measured for wild type and ClC3 or ClC5 knockout animals at sacrifice (Fig. 4). In keeping with effects on bone formation, ClC3 knockout mice, males and females had ~15 %, and significantly, lower weights than controls (Fig. 4A). Surprisingly, at 5 months, body weights of ClC5 knockout female were ~10 % higher than control mice ($p = 0.01$), although there were not significant changes in ClC5 deficient male mice (Fig. 4B). Serum ALP (Fig. 4C) and TRAP (Fig. 4D) both showed high variability and overlap between wild type and knockouts. However, alkaline phosphatase was significantly lower in the ClC5 animals ($p = 0.02$). Direct labeling of osteoclasts by tartrate

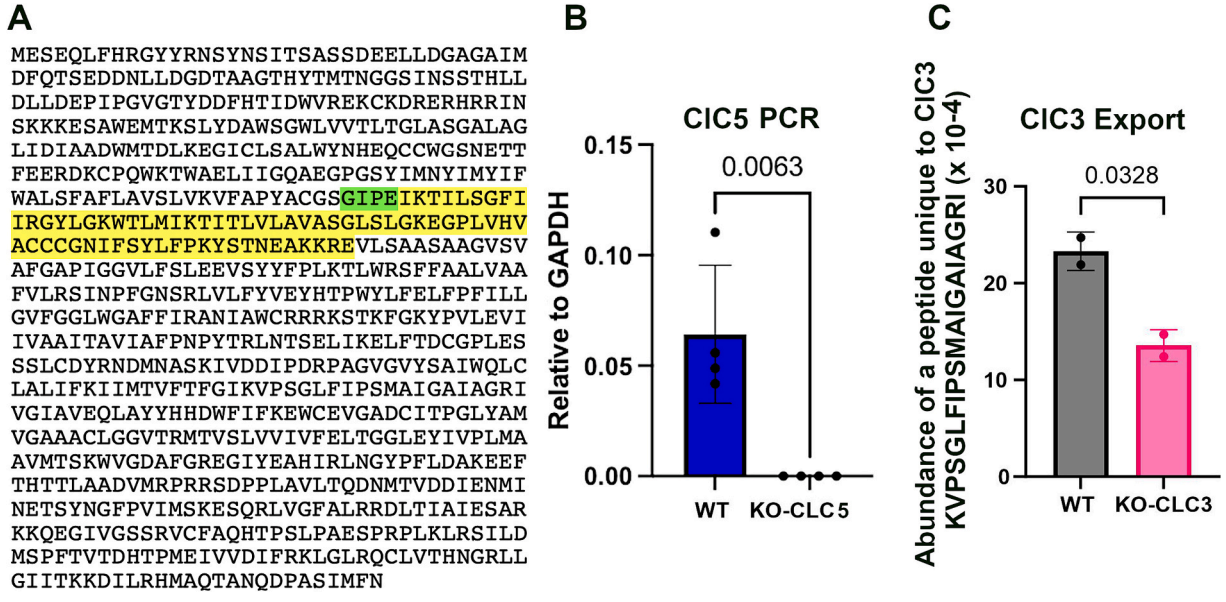

Fig. 1. The ClC3 functional knockout and the ClC5 knockout.

A. Sequence of ClC3 showing deleted amino acids in the functional knockout. Amino acids deleted in ClC3 are in green (end of exon 6) and yellow (exon 7) by total exon sequencing. The ClCN3 functional knockout had been characterized by PCR and Southern analysis; amino acid sequencing had not previously been performed. The deletion is as expected from the original mouse (Dickerson et al., 2002) despite many generations of breeding and changing the host to C57black.

B. The ClC5 knockout produces no ClC5 protein. Amount of ClC 5 produced in wild type and knockout animals. This was also done using stromal stem cells, with identical results (not shown).

C. Expression of ClC3 protein is reduced in the ClC3 functional knockout. We compared abundance of a unique peptide in the wild type and ClC3 knockout in osteoblasts from stromal stem cells, by mass spectrometry for a peptide unique to ClC3. This confirmed the PCR result (Larrouture et al., 2015) that the protein is exported in the knockout, albeit with ~40 % reduction of the wild type quantity.

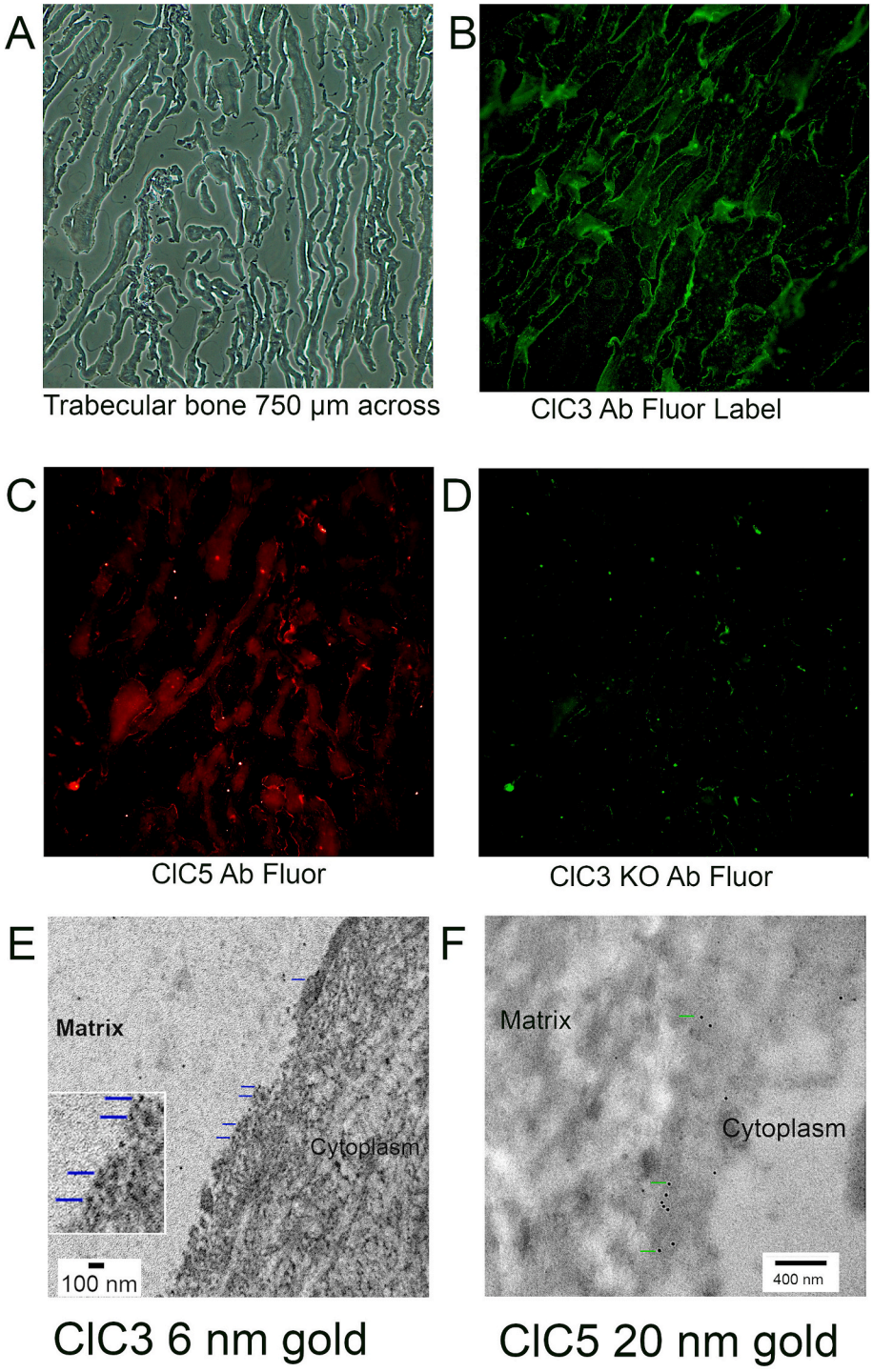

Fig. 2. Localization of ClC5 and of ClC3 to the matrix surface of osteoblasts.
A-D. Antibody fluorescence labeling of bone trabeculae for ClC3 and ClC5. Each frame is 750 μm across. **(A)** Trabecular structure at this power is shown at the top left in phase contrast. **(B)** Strong labeling of ClC3 and **(C)** slightly less labeling of ClC5 at borders of trabeculae, in young wild type mice (12 weeks). **(D)** Knockout bone using antibody to the internal epitope missing in the ClC3 knockout (Methods and Fig. 2) does not label ClC3. Both the wild type and ClC3 knockout proteins are exported, although somewhat less in the ClC3 knockout, (see Fig. 1C).
E-F. Antibody-gold labeling of ClC3 (left) and ClC5 (right) at the cytoplasm-matrix interface. Some of the gold indicated by green lines. In the ClC3, gold is 6 nm seen at high power (bar is 100 nm). For clarity, an insert in Fig. 3E shows part of the surface with gold at twice the magnification. The ClC5 is labeled with 20 nm gold and is seen at lower magnification (bar 400 nm).

resistant acid phosphatase near growth plates of wild type, ClC3 knockout, and ClC5 knockout showed similar osteoclast formation (Fig. 4E). While this method is not suitable for detailed quantitative analysis, relative to wild type (Fig. 4E, left) labeled cells in the ClC3 knockout were consistent with greater TRAP in serum (Fig. 4D), and apparent bone area in the ClC5 knockout (Fig. 4E, right) was consistent with greater average animal weights (Fig. 4A and B). Nuclear labeling by 4′,6-diamidino-2-phenylindol (DAPI) showed no meaningful differences and is not illustrated.

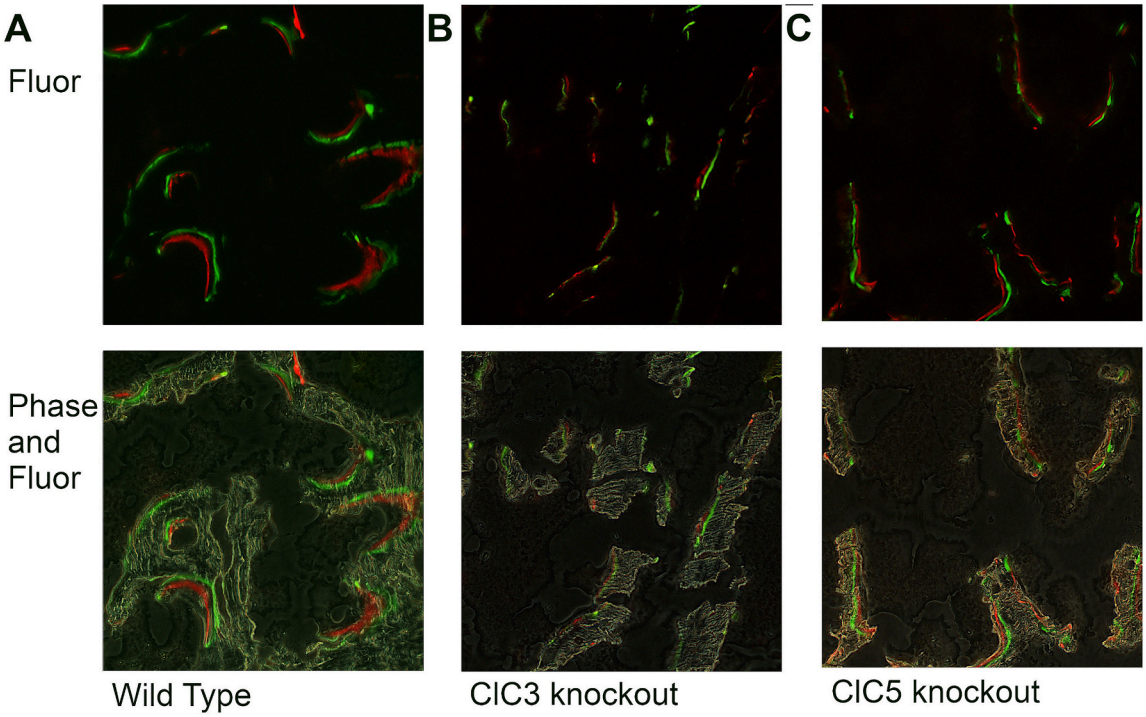

D. Labeled area per trabecular surface (dimensionless)

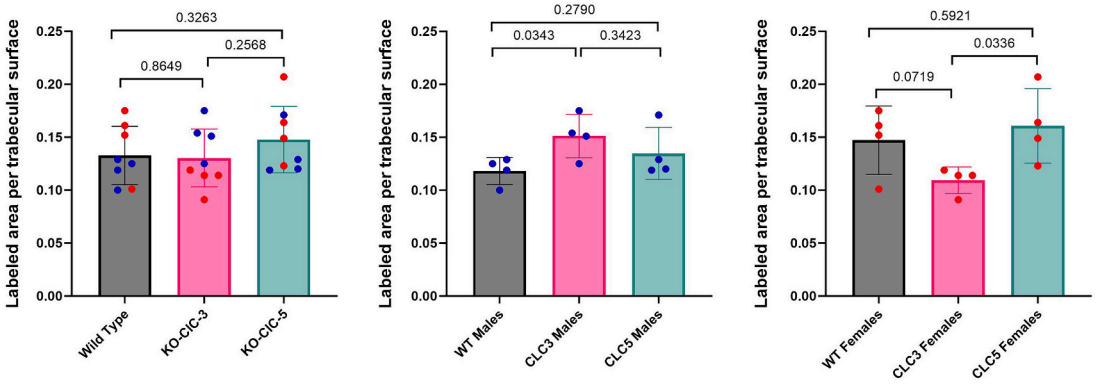

E. Interlabel distance (microns)

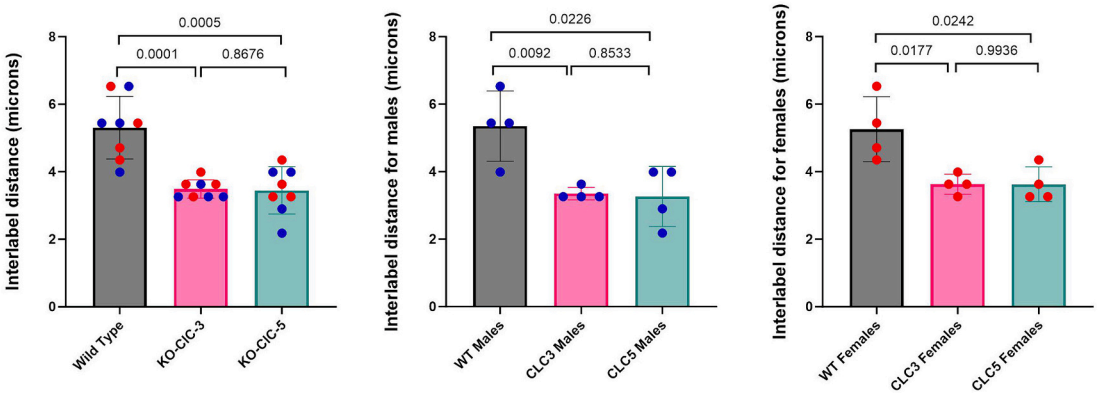

(caption on next page)

Fig. 3. Bone formation in ClC3 and ClC5 knockout mice.
A-C. Effect on calcein and xylenol orange labeling in representative bone sections. A minimum of four animals of each genotype were labeled using calcein IP on day 1, xylenol orange IP on day 4, and sacrifice on day 6, sections were cut and analyzed. The sections shown are 450 μm wide. In each case, the top frame shows the calcein label in green and xylenol orange in red; the bottom frame shows the same labels superimposed on a phase image of the trabecular bone at the same site.
D-E. Effect on quantitative calcein and xylenol orange labeling. In each case, the left graph shows males (blue) and females (red) superimposed. The middle graph is for males only, the right graph females only.
D. Labeled area as percent of bone surface. There are interesting differences but all are quantitatively small, and the only ones significant are slight but significant increase in labeled area in $ClC3^{-/-}$ males relative to wild type (middle graph) and decreased labeled area in $ClC3^{-/-}$ females relative either wild type or ClC5 knockouts (right graph).
E. Interlabel distance in microns. Detailed μCT showed effects of the ClC5 and ClC3 knockout on interlabel distance were both significantly reduced ($p = 0.01$ to 0.02), and by about 30 % in either males or females. These findings were remarkably consistent between the ClC3 and ClC5 knockouts.

3.5. Detailed static histomorphometry by micro-computed tomography

Calcein and xylenol orange showed significant reduction in bone apposition, changing the trabecular thickness, for both ClC3 and ClC5 knockouts, on careful measurement at high magnification (Fig. 3A-C, E). This occurred with variable changes in labeled surface (Fig. 3D) and variable animal weight, sex, serum alkaline phosphatase and TRAP (Fig. 4). Therefore, we also studied 2–3 times as many animals and analyzed major histomorphometric parameters for bone by micro-computed tomography. The larger numbers allow quantitative comparisons of major quantitative parameters between the wild type, ClC3 and ClC5 knockout genotypes despite variability in sex and weight (Fig. 4).

Comparisons of vertical sections of wild type, ClC3 knockout, and ClC5 knockout are shown (Fig. 5A,B,C). The change in ClC3 knockout density is clear relative to wild type (Fig. 5A relative to Fig. 5B), with less bone less well connected in the ClC3 knockout. Differences from wild type in the ClC5 knockout are less obvious (Fig. 5C) on direct examination.

Quantitative data analysis showed changes in ClC5 knockout animals relative to the wild type, generally intermediate between the wild type and ClC3 knockout. Both ClC3 and ClC5 knockout animals had decreased bone volume/total volume relative to the wild type (Fig. 5D). Decreased labeling in Fig. 5D was better resolved blinded by calcein and xylenol orange labeling in the ClC5 knockouts (Fig. 3). On the other hand, only the ClC3 knockout affected the intersection surface, with a 40 % decrease (Fig. 5E). Both the ClC3 and ClC5 knockouts had increased porosity, mainly affecting the ClC5 knockout males (Fig. 5F), with very high variability in the ClC5 knockout. Not surprisingly the trabecular thickness was decreased in the ClC3 knockout (Fig. 5G); there was a small, but significant, decrease in the ClC5 knockout. The spacing between trabeculae (trabecular number per cm) is determined by trabecular separation from cartilaginous growth plates, and not surprisingly, did not change significantly (Fig. 5H). The large decrement in apposition (bone formation, Fig. 3) in the ClC3 knockout leads to an increment in bone surface/bone volume (Fig. 5I). The small but significant effect on trabecular thickness in the ClC5 knockout (Fig. 5G) corresponds to a significant increase relative to wild type in the bone surface/bone volume (Fig. 5I, right bar).

3.6. Effects on the kidney and teeth

In keeping with previous reports on ClC5 deficiency, also called Dent's disease, ClC5 knockout animals had in addition renal and bladder abnormalities and dental defects, previously attributed to stone formation (Jentsch, 2005), and abnormal tooth growth also previously reported in mice (Duan et al., 2009). Since our focus is on bone formation, these are not further evaluated or discussed but are illustrated (Supplemental Fig. 3).

4. Discussion

In growing mouse bone, ClC3 and, to a lesser extent, ClC5 are highly expressed (Larrouture et al., 2015), and found at least in part at the plasma membrane-matrix interface (Fig. 2). The ClC proteins, of which there are many, are important in a variety cells for a multiple purposes. As an example, weakly outward-rectifying ClC3 is reported in the cell surface of a nasopharangeal cancer cell line (Zheng et al., 2019). Contrariwise, the transporters ClC3 through ClC7 are generally regarded as mainly intracellular and strongly rectifying, with complex localization particular to the endosomal-lysosomal pathway (Bose et al., 2021). However, with tissue-specific expression they may function as $2Cl^-/H^+$ exchangers or as chloride channels.

Many defects in ClC3 are known, and are associated with neurodegenerative diseases in humans (Duncan et al., 2021). Function of a ClC3 expression variant as a cell-surface exchanger is also reported (Robinson et al., 2004). Expression of ClC3 in additional tissues is reported, without detailed characterization; this includes possible function in intestinal epithelium (Claud et al., 2008). In contrast, the association of ClC5 defects with specific kidney defects (Dent disease) is extensively described, although ClC5 is regarded as mainly endosomal (Zifarelli, 2015), ClC5 plasma membrane distribution is described (Sakhi et al., 2021).

In the bone, effects of ClC3 were also studied by *in vitro* analysis of osteoclast differentiation and function (Okamoto et al., 2008), who showed reduced osteoclast formation and function on the order of 30 %. Interestingly, in our *in vivo* work, osteoclasts at the growth plates in the spine were similar in wild type and ClC3 or ClC5 knockouts (Fig. 4E), and serum TRAP was moderately increased in ClC3 knockout animals (Fig. 4D). There was no evidence of osteopetrosis; this is not surprising because bone resorption is subject to multiple types of feedback regulation. This will be an interesting topic for further study.

More directly, we isolated osteoblast cell membranes with nitrogen cavitation and reconstitution of vesicles (Blair et al., 2018). This showed Cl^- dependent H^+ uptake in vesicles (Blair et al., 2018). This suggested strongly an atypical function of ClCs in osteoblasts. However, it is highly likely that ClC3 in the osteoblast is part of a complex mechanism, including also almost certainly other proteins linked to ClC3 currently unknown. ClCs form dimers and heterodimers (Stauber et al., 2012), and are PDZ binding proteins (Gentzsch et al., 2003). This will require separate investigation.

We hypothesize that in the growing bone, ClC3 and ClC5 function as H^+/Cl^- transporters in the important movement of H^+ out of forming bone mineral (Fig. 6). In addition to documenting the unusual distribution of ClC3 and ClC5 at the osteoblast-matrix interface (Fig. 2), we did detailed characterization of the ClC3 functional knockout in osteoblasts. This included comparing abundance of a unique peptide in the wild type and ClC3 knockout in osteoblasts from stromal stem cells by mass spectrometry (Fig. 1). This confirmed our PCR result (Larrouture et al., 2015) that the protein is produced in the knockout, albeit with ~40 % reduction of quantity (Fig. 1C). Reduced protein quantity is a common finding for proteins the structure of which is modified, although the missing segment does not cause termination. By Western analysis, the two proteins gave similar results, wild type and knockout (not illustrated). However, (Dickerson et al., 2002) were able to distinguish the molecular weights of the ClC3 wild type and conditional knockout by high-resolution electrophoretic separation.

The ClC3 and ClC5 knockouts were not clearly related to the main serum proteins that indicate bone turnover, the LKB alkaline

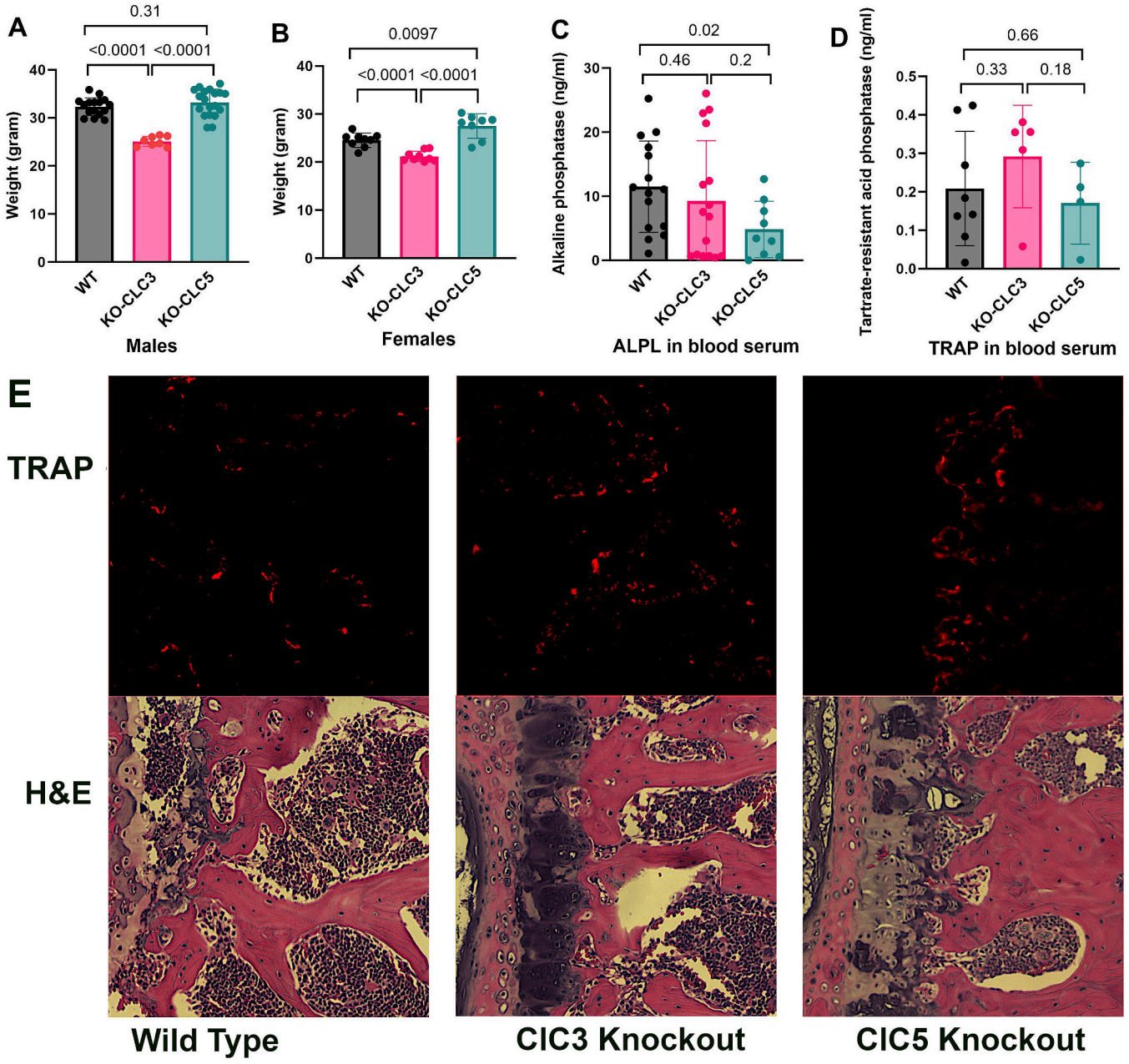

Fig. 4. Weights and serum chemistry knockout mice. Recorded in 5 month animals, males and females of wild type and ClC3 or ClC5 knockouts.
A. Weights of wild type *versus* ClC3 and ClC5 knockout animals, Males. Knockout ClC3 animals, male or female, were 15–20 % reduced on average, with $p <$ 0.001 in both cases.
B. Weights of wild type *versus* ClC3 and ClC5 knockout animals, Females. Females were ~ 15 % lighter than males but the pattern was the same as in males.
C. Serum Alkaline Phosphatase in Wild Type and ClC3 or ClC5 knockout Mice. Alkaline phosphatase in serum was reduced in the ClC5 knockout, although variability was high with significant overlap.
D. Serum TRAP in Wild Type and ClC3 or ClC5 knockout Mice. TRAP did not change significantly relative to wild type in either knockout.
E. Sections, 420 μm square, adjacent to the growth plate antibody labeled for TRAP. On the top is direct labeling of tartrate resistant acid phosphatase near growth plates of wild type. On the bottom, an adjacent section from the same animal in hematoxylin and eosin (H&E) showing bone and marrow. This method is qualitative. However, relative to wild type (left frame) labeled cells in the ClC3 knockout (middle frame) were consistent with greater TRAP in serum (Panel D). Bone mass in the ClC5 knockout (right frame) was consistent with greater average animal weights (Panels A and B).

phosphatase, reduced with decreased bone formation (López-Delgado et al., 2018) and tartrate-resistant acid phosphatase, an indicator of osteoclast activity (Henriksen et al., 2007). Serum alkaline phosphatase (Fig. 4C) and TRAP (Fig. 4D) had high variability and both showed overlap between wild type and knockouts. While alkaline phosphatase was reduced in the ClC5 animals, there was overlap and variability. The bone resorption marker, TRAP, did not change significantly in knockout animals. Possible differences in ClC5 with reduced serum alkaline phosphatase and TRAP are regarded as insufficient for definite conclusions. However, overall the data suggest that ClC3 and ClC5 do not affect these enzymes, involved in bone formation and resorption, in any major way. Indeed, direct labeling of osteoclasts in tissue showed normal formation at bone-forming growth plates in the spine (Fig. 4E). There are probably differences in resorption reflected in density of bone and other parameters (Fig. 5) but current work cannot resolve differences in bone resorption, despite showing that osteoclasts form normally in the

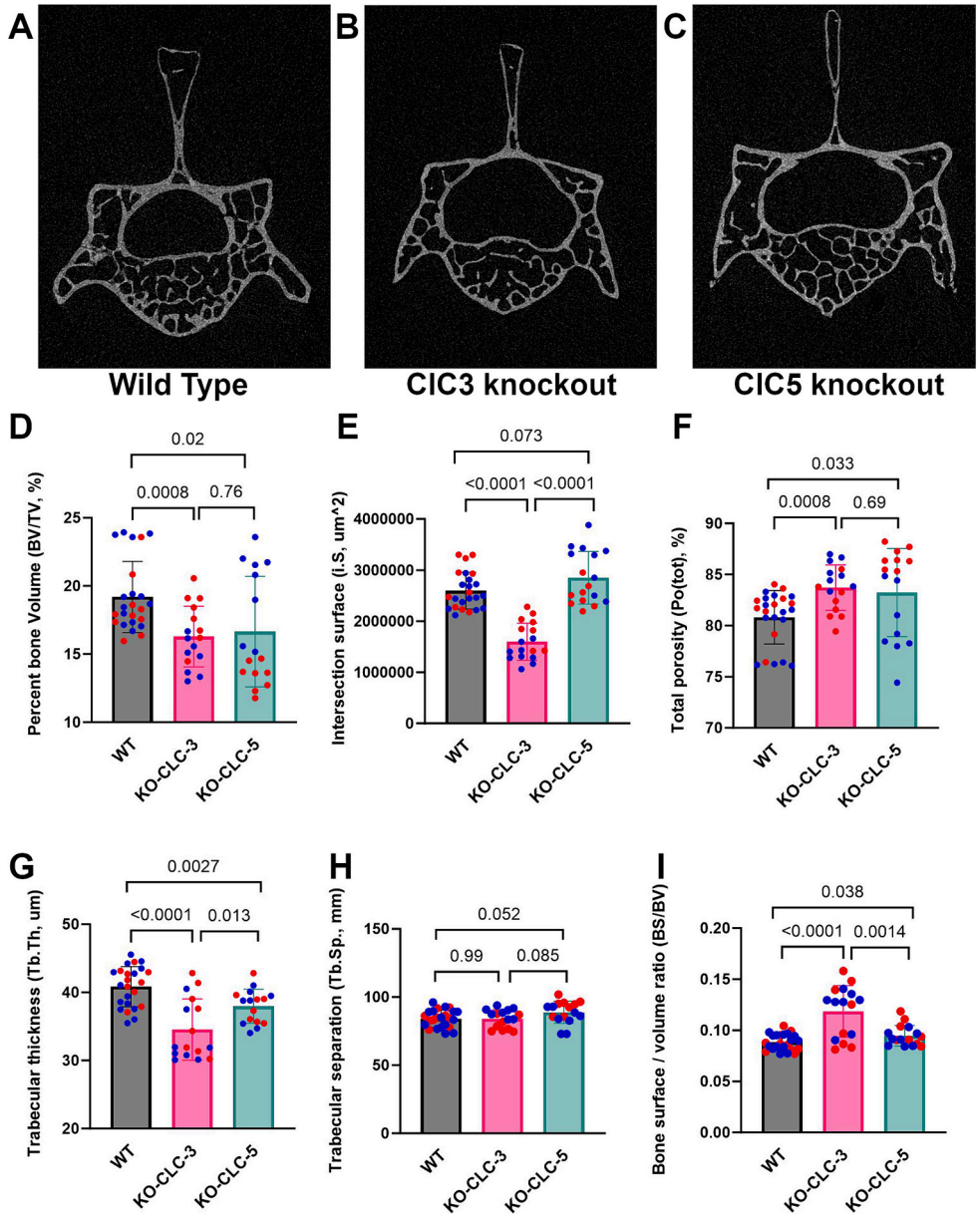

Fig. 5. Effect of ClC3 and ClC5 knockout on bone structure. A-C shows vertical sections of wild type, ClC3 knockout, and ClC5 knockout mice. D-I show micro-computed tomography: In each case, the left bar is wild type, $ClC3^{-/-}$ is the middle bar, in red, and $ClC5^{-}$ (males) or $^{-/-}$ (females) are shown in the right bar (green). In each bar, for individual data points males are blue dots and females are red dots.

A. Vertical section through L4 of the wild type mouse.

B. Vertical section through L4 of the $ClC3^{-/-}$ animal. The density of bone is clearly less than wild type of ClC5 knockout

C. Vertical section through L4 of the $ClC5^{-/-}$ (male) animal. The difference in bone density with wild type (A) is not clear by visual examination.

D. Bone volume/Total volume, %. This is reduced in both knockouts about 30 % on average relative to the wild type; difference in this parameter between ClC3 and ClC5 is not significant.

E. Intersection Surface, μm^2. This is reduced on average relative to the wild type about 40 % in the ClC3 only. This is marginally increased relative to the wild type in ClC5 knockouts.

F. Total Porosity. This is increased by a small amount in both knockouts.

G. Trabecular Thickness. This is decreased in both knockouts, more in the ClC3 knockout.

H. Trabecular number per cm. This is unaffected by the knockouts, in keeping with trabecular formation involving different mechanisms than growth.

I. Bone Surface/Bone Volume. This is increased in the ClC3 knockout and to a minor extent in the ClC5 knockout, on average.

wild type and ClC3 or ClC5 knockouts.

ClC3 knockout mice are osteopenic relative to the WT mice. This is in keeping with a role for ClC3 in transport of bone mineral, particularly of H^+. Both ClC3, and to a lesser extent ClC5, occur at the osteoblast-matrix interface in wild type mice (Fig. 2). Earlier we reported that ClC5 is upregulated in ClC3 knockout mice (Larrouture et al., 2015), suggesting that ClC5 may have a role in transport relative to ClC3, possibly with the ClC3 and ClC5 regulated relative between each other in bone. Our findings that ClC5 knockout impaired bone formation is in keeping with this hypothesis. In our previous work, expression of ClC5 was about 20 % relative to expression of ClC3 by PCR and Western blots (Larrouture et al., 2015), in keeping with the relative labeling by fluorescent antibodies (Fig. 2BC).

The percent bone surface with fluorescent label showed fairly small

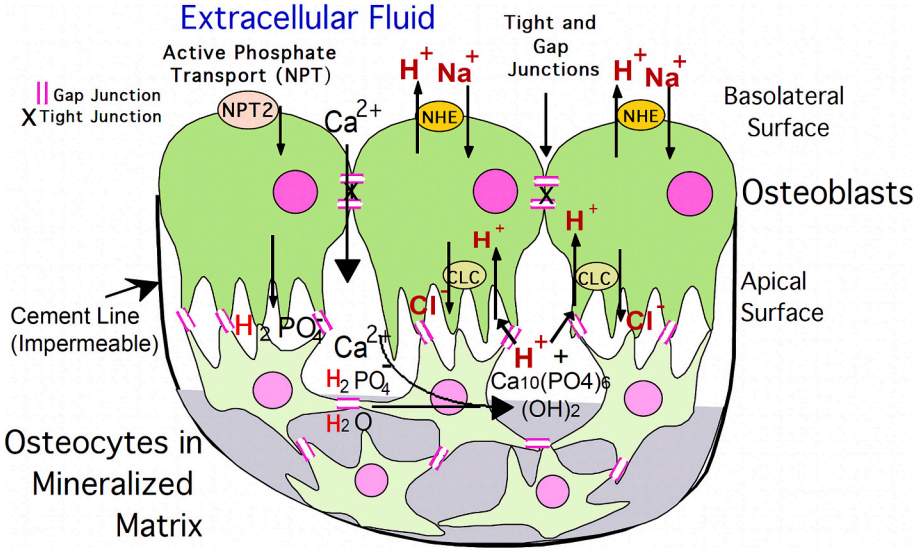

Fig. 6. Mineral formation in osteoblasts is hypothesized to depend on H^+/Cl^- exchange. A model of the hypothesis tested here, that when phosphate is converted to hydroxyapatite with evolution of acid, the acid is removed from the bone by an ion transport mechanism that depends on ClC proton-chloride exchangers, at least in part. The work here shows functional importance of both ClC3 and ClC5. Beyond this, the phosphate is transported by active transport (neutral phosphate transporter 2) and the calcium by passive transport (intercellular). Once acid is taken up by osteoblasts, its removal is by basolateral sodium hydrogen exchangers (NHEs).

differences between the control and either knockout animal (Fig. 3D). But, there was a large decrease in bone formation rate in either the ClC3 or ClC5 knockout. This leads to an important question: if, for example, the ClC3 protein is critical for bone transport in osteoblasts, then in theory the ClC3 knockout animals should produce no bone. This does not occur: The bone production decreases about 40 % as derived from the interlabel distance of calcein and xylenol orange labeling (Fig. 3D), so at least one other mechanism must be present if the hypothesis regarding ClC activity and bone formation is, in major part, correct. That the same is seen with ClC5. The knockout reduces but does not abolish bone apposition (Fig. 3D). This suggests that the two transporters both function, at least in part, in parallel. This is the most obvious connection with the fatal outcome of the double knockout – with neither transporter vital functions are disrupted. However, since the transporters are expressed in many tissues, at this point this is completely hypothetical.

This was supported by highly sensitive micro computed tomography measurements, done blindly and where it is practical to analyze many more animals, showing overlapping activity of ClC5 and ClC3 (Fig. 5). The ClC5 animals showed changes in bone morphometry, different from those in ClC3 knockout mice, but with the major effects being similar. Specifically, bone volume/total volume was reduced in the ClC5 knockout relative to control mice by an amount similar to the ClC3 knockout result. (Fig. 5D). Total porosity was increased in ClC5 knockout mice relative to the wild type (Fig. 5F), by an amount intermediate between the wild type and ClC3 knockout. Trabecular thickness in ClC5 knockout mice was reduced relative to the wild type (Fig. 5G), again, intermediate with the effects of the ClC3 knockout, with both differences being significant (for *p*-values see Fig. 5G). The bone surface/bone volume was also intermediate in the ClC5 knockout between the wild type and ClC3 knockout (Fig. 5I), by small, but significant, amounts. Essentially invariant measurements included trabecular separation. The trabeculae are formed by alignment of cells at growth plates, not involved in mineralization of bone. In keeping with this, differences between the wild type and the ClC3 or ClC5 knockout trabecular separation (Fig. 5H) were small and not significant.

Since it proved impossible to produce a ClC3-ClC5 double knockout. we hypothesize that with both transporters absent, very little bone might be made. Since the transporters are not bone-specific, full workup of this hypothesis will require conditional knockouts of ClC3 or ClC5 that would be specific for bone. Future work will focus on this, using cre/flox technology (Horii et al., 2017). We will also study ClC5 knockout, $ClC3^{+/-}$ animals. This may provide additional support for interaction of the two ClC proteins until additional studies are available.

Animal weights at 5 months showed that ClC3 knockout mice, males and females had 15 %, and significantly, lower weights than controls (Fig. 4A), in keeping with reduced bone growth (Fig. 3). Body weight of ClC5 knockout female was ~10 % higher than WT mice ($p = 0.01$), with no significant changes in ClC5 knockout male mice relative to the wild type. Since CLC knockouts are expressed in multiple tissues, this variation is not surprising. Additional parameters that bear further investigation include possible changes in bone quality with gonadectomy and PTH, and further blood chemistry including calcium and phosphorus in addition to the limited studies of alkaline phosphatase and TRAP, Fig. 4. Indeed, detailed study of body composition would be justified, as the antiporters may affect whole body metabolism or energy balance.

We conclude that both ClC3 and ClC5 contribute to bone formation, with similar importance to bone formation overall. Fig. 6 illustrates the central hypothesis.

Supplementary data to this article can be found online at https://doi.org/10.1016/j.bonr.2024.101763.

CRediT authorship contribution statement

Irina L. Tourkova: Investigation, Methodology, Project administration, Supervision, Validation, Writing – original draft, Writing – review & editing. **Quitterie C. Larrouture:** Investigation, Methodology, Validation, Writing – original draft. **Silvia Liu:** Data curation, Formal analysis, Methodology, Writing – original draft. **Jianhua Luo:** Conceptualization, Methodology, Supervision, Visualization. **Katherine E. Shipman:** Data curation, Formal analysis, Investigation, Methodology, Writing – review & editing. **Kelechi M. Onwuka:** Investigation, Validation. **Ora A. Weisz:** Conceptualization, Funding acquisition, Investigation, Methodology, Supervision, Writing – review & editing. **Vladimir Riazanski:** Formal analysis, Investigation, Writing – original draft. **Deborah J. Nelson:** Conceptualization, Formal analysis, Funding acquisition, Investigation, Project administration, Supervision, Writing – review & editing. **Matthew L. MacDonald:** Formal analysis, Investigation, Methodology, Validation, Writing – original draft. **Paul H.**

Schlesinger: Conceptualization, Funding acquisition, Investigation, Methodology, Visualization, Writing – original draft, Writing – review & editing. **Harry C. Blair:** Conceptualization, Data curation, Formal analysis, Funding acquisition, Investigation, Methodology, Project administration, Supervision, Validation, Writing – original draft, Writing – review & editing.

Declaration of competing interest

All of the authors declare no financial and personal relationships with people or organizations that might inappropriately influence the work. No author is under investigation for responsible conduct in research, animal welfare, human subjects, or laboratory safety compliance at the time of submission.

Data availability

The sequence data reported in this article are deposited in the National Institutes of Health (USA) Sequence Read Archive PRJNA1064390. Raw FASTQ files can be downloaded at: https://www.ncbi.nlm.nih.gov/bioproject/PRJNA1064390. Other research data and metadata are deposited in our cloud-based institutional database, https://d-scholarship.pitt.edu. This is the institutional repository for research of the University of Pittsburgh, indexed under Orcid 0000-0002-1152-3718.

Acknowledgements

Supported in part by USA NIH grants AR076146 (HCB and PHS) DK125049 (OW) and DK121394 (KES), and by BX002490-06A1 from the United States Department of Veteran's Affairs (HCB).

References

Blair, H.C., Larrouture, Q.C., Tourkova, I.L., Liu, L., Bian, J.H., Stolz, D.B., Nelson, D.J., Schlesinger, P.H., 2018. Support of bone mineral deposition by regulation of pH. Am. J. Physiol. Cell Physiol. 2018 (315), C587–C597. https://doi.org/10.1152/ajpcell.00056.2018.

Blair, H.C., Larrouture, Q.C., Tourkova, I.L., Nelson, D.J., Dobrowolski, S.F., Schlesinger, P.H., 2023. J. Cell. Biochem. 124, 1889–1899. https://doi.org/10.1002/jcb.30494.

Bose, S., He, H., Stauber, T., 2021. Neurodegeneration upon dysfunction of endosomal/lysosomal CLC chloride transporters. Front. Cell Dev. Biol. 9, 639231 https://doi.org/10.3389/fcell.2021.639231.

Claud, E.C., Lu, J., Wang, X.Q., Abe, M., Petrof, E.O., Sun, J., Nelson, D.J., Marks, J., Jilling, T., 2008. Platelet-activating factor-induced chloride channel activation is associated with intracellular acidosis and apoptosis of intestinal epithelial cells. Am. J. Physiol. Gastrointest. Liver Physiol. 294, G1191–G1200. https://doi.org/10.1152/ajpgi.00318.2007.

Dickerson, L.W., Bonthius, D.J., Schutte, B.C., Yang, B., Barna, T.J., Bailey, M.C., Nehrke, K., Williamson, R.A., Lamb, F.S., 2002. Altered GABAergic function accompanies hippocampal degeneration in mice lacking ClC-3 voltage-gated chloride channels. Brain Res. 958, 227–250. https://doi.org/10.1016/s0006-8993(02)03519-9.

Duan, X., Mao, Y., Yang, T., Wen, X., Wang, H., Hou, J., Xue, Y., Zhang, R., 2009. ClC-5 regulates dentin development through TGF-beta1 pathway. Arch. Oral Biol. 54, 1118–1124. https://doi.org/10.1016/j.archoralbio.2009.09.008.

Duncan, A.R., Polovitskaya, M.M., Gaitán-Peñas, H., Bertelli, S., VanNoy, G.E., Grant, P. E., O'Donnell-Luria, A., Valivullah, Z., Lovgren, A.K., England, E.M., Agolini, E., Madden, J.A., Schmitz-Abe, K., Kritzer, A., Hawley, P., Novelli, A., Alfieri, P., Colafati, G.S., Wieczorek, D., Platzer, K., Agrawal, P.B., 2021. Unique variants in CLCN3, encoding an endosomal anion/proton exchanger, underlie a spectrum of neurodevelopmental disorders. Am. J. Hum. Genet. 108, 1450–1465. https://doi.org/10.1016/j.ajhg.2021.06.003.

Gentzsch, M., Cui, L., Mengos, A., Chang, X.B., Chen, J.H., Riordan, J.R., 2003. The PDZ-binding chloride channel ClC-3B localizes to the Golgi and associates with cystic fibrosis transmembrane conductance regulator-interacting PDZ proteins. J. Biol. Chem. 278, 6440–6449. https://doi.org/10.1074/jbc.M211050200.

Henriksen, K., Tanko, L.B., Qvist, P., Delmas, P.D., Christiansen, C., Karsdal, M.A., 2007. Assessment of osteoclast number and function: application in the development of new and improved treatment modalities for bone diseases. Osteoporos. Int. 18, 681–685. https://doi.org/10.1007/s00198-006-0286-8.

Horii, T., Morita, S., Kimura, M., Terawaki, N., Shibutani, M., Hatada, I., 2017. Efficient generation of conditional knockout mice via sequential introduction of lox sites. Sci. Rep. 7, 7891. https://doi.org/10.1038/s41598-017-08496-8.

Jentsch, T.J., 2005. Chloride transport in the kidney: lessons from human disease and knockout mice. J. Am. Soc. Nephrol. 216, 1549–1561. https://doi.org/10.1681/ASN.2005020207.

Larrouture, Q.C., Nelson, D.J., Robinson, L.J., Liu, L., Tourkova, I., Schlesinger, P.H., Blair, H.C., 2015. Chloride-hydrogen antiporters ClC-3 and ClC-5 drive osteoblast mineralization and regulate fine-structure bone patterning in vitro. Physiol. Rep. 3, e12607 https://doi.org/10.14814/phy2.12607.

Larrouture, Q.C., Tourkova, I.L., Stolz, D.B., Riazanski, V., Onwuka, K.M., Franks, J.M., Dobrowolski, S.F., Nelson, D.J., Schlesinger, P.H., Blair, H.C., 2021. Growth and mineralization of osteoblasts from mesenchymal stem cells on microporous membranes: epithelial-like growth with transmembrane resistance and pH gradient. Biochem. Biophys. Res. Commun. 580, 14–19. https://doi.org/10.1016/j.bbrc.2021.09.075.

Liu, L., Schlesinger, P.H., Slack, N.M., Friedman, P.A., Blair, H.C., 2011. High capacity Na^+/H^+ exchange activity in mineralizing osteoblasts. J. Cell. Physiol. 226, 1702–1712. https://doi.org/10.1002/jcp.22501.

Liu, L., Alonso, V., Guo, L., Tourkova, I., Henderson, S.E., Almarza, A.J., Friedman, P.A., Blair, H.C., 2012. Na+/H+ exchanger regulatory factor 1 (NHERF1) directly regulates osteogenesis. J. Biol. Chem. 287, 43312–43321. https://doi.org/10.1074/jbc.M112.422766.

López-Delgado, L., Riancho-Zarrabeitia, L., García-Unzueta, M.T., Tenorio, J.A., García-Hoyos, M., Lapunzina, P., Valero, C., Riancho, J.A., 2018. Abnormal bone turnover in individuals with low serum alkaline phosphatase. Osteoporos. Int. 29, 2147–2150. https://doi.org/10.1007/s00198-018-4571-0.

McGuffin, L.J., Edmunds, N.S., Genc, A.G., Alharbi, S.M.A., Salehe, B.R., Adiyaman, R., 2023. Prediction of protein structures, functions and interactions using the IntFOLD7, MultiFOLD and ModFOLDdock servers. Nucleic Acids Res. 51 (W1), W274–W280. https://doi.org/10.1093/nar/gkad297.

Okamoto, F., Kajiya, H., Toh, K., Uchida, S., Yoshikawa, M., Sasaki, S., Kido, M.A., Tanaka, T., Okabe, K., 2008. Intracellular ClC-3 chloride channels promote bone resorption in vitro through organelle acidification in mouse osteoclasts. Am. J. Physiol. Cell Physiol. 294, C693–C701. https://doi.org/10.1152/ajpcell.00251.2007.

Puig, S., Xue, X., Salisbury, R., Shelton, M.A., Kim, S.M., Hildebrand, M.A., Glausier, J.R., Freyberg, Z., Tseng, G.C., Yocum, A.K., Lewis, D.A., Seney, M.L., MacDonald, M.L., Logan, R.W., 2023. Circadian rhythm disruptions associated with opioid use disorder in synaptic proteomes of human dorsolateral prefrontal cortex and nucleus accumbens. Mol. Psychiatry 28, 4777–4792. https://doi.org/10.1038/s41380-023-02241-6.

Robinson, N.C., Huang, P., Kaetzel, M.A., Lamb, F.S., Nelson, D.J., 2004. Identification of an N-terminal amino acid of the CLC-3 chloride channel critical in phosphorylation-dependent activation of a CaMKII-activated chloride current. J. Physiol. 556 (Pt 2), 353–368. https://doi.org/10.1113/jphysiol.2003.058032.

Robinson, L.J., Soboloff, J., Tourkova, I.L., Larrouture, Q.C., Onwuka, K.M., Papachristou, D.J., Gross, S., Hooper, R., Samakai, E., Worley, P.F., Liu, P., Tuckermann, J., Witt, M.R., Blair, H.C., 2023. The calcium channel Orai1 is required for osteoblast development: studies in a chimeric mouse with variable in vivo Runx-cre deletion of Orai-1. PloS One 18, e0264596. https://doi.org/10.1371/journal.pone.0264596.

Rohrbough, J., Nguyen, H.N., Lamb, F.S., 2018. Modulation of ClC-3 gating and proton/anion exchange by internal and external protons and the anion selectivity filter. J. Physiol. 596, 4091–4119. https://doi.org/10.1113/JP276332.

Sakhi, I., Bignon, Y., Frachon, N., Hureaux, M., Arévalo, B., González, W., Vargas-Poussou, R., Lourdel, S., 2021. Diversity of functional alterations of the ClC-5 exchanger in the region of the proton glutamate in patients with dent disease 1. Hum. Mutat. 42, 537–550. https://doi.org/10.1002/humu.24184.

Salazar, G., Love, R., Styers, M.L., Werner, E., Peden, A., Rodriguez, S., Gearing, M., Wainer, B.H., Faundez, V., 2004. AP-3-dependent mechanisms control the targeting of a chloride channel (ClC-3) in neuronal and non-neuronal cells. J. Biol. Chem. 279, 25430–25439. https://doi.org/10.1074/jbc.M402331200.

Schlesinger, P.H., Braddock, D.T., Larrouture, Q.C., Ray, E.C., Riazanski, V., Nelson, D.J., Tourkova, I.L., Blair, H.C., 2020. Phylogeny and chemistry of biological mineral transport. Bone 141, 115621. https://doi.org/10.1016/j.bone.2020.115621.

Shipman, K.E., Baty, C.J., Long, K.R., Rbaibi, Y., Cowan, I.A., Gerges, M., Marciszyn, A. L., Kashlan, O.B., Tan, R.J., Edwards, A., Weisz, O.A., 2023. Impaired endosome maturation mediates tubular proteinuria in dent disease cell culture and mouse models. J. Am. Soc. Nephrol. 34, 619–640. https://doi.org/10.1681/ASN.0000000000000084.

Stauber, T., Weinert, S., Jentsch, T.J., 2012. Cell biology and physiology of CLC chloride channels and transporters. Compr. Physiol. 2, 1701–1744. https://doi.org/10.1002/cphy.c110038.

Tourkova, I.L., Liu, L., Sutjarit, N., Larrouture, Q.C., Luo, J., Robinson, L.J., Blair, H.C., 2017. Adrenocorticotropic hormone and 1,25-dihydroxyvitamin D3 enhance human osteogenesis in vitro by synergistically accelerating the expression of bone-specific genes. Lab. Invest. 97, 1072–1083. https://doi.org/10.1038/labinvest.2017.62.

Tourkova, I.L., Larrouture, Q.C., Onwuka, K.M., Liu, S., Luo, J., Schlesinger, P.H., Blair, H.C., 2023. Age-related decline in bone mineral transport and bone matrix

proteins in osteoblasts from stromal stem cells. Am. J. Physiol. Cell Physiol. 325, C613–C622. https://doi.org/10.1152/ajpcell.00227.2023.

Zheng, Y., Chen, Z., Gu, Z., Yang, X., Yu, M., Zhao, C., Lin, J., Xu, P., Zhu, L., Jacob, T.J. C., Peng, S., Chen, L., Wang, L., 2019. Starvation-induced autophagy is up-regulated via ROS-mediated ClC-3 chloride channel activation in the nasopharyngeal carcinoma cell line CNE-2Z. Biochem. J. 476, 1323–1333. https://doi.org/10.1042/BCJ20180979.

Zifarelli, G., 2015. A tale of two CLCs: biophysical insights toward understanding ClC-5 and ClC-7 function in endosomes and lysosomes. J. Physiol. 593, 4139–4150. https://doi.org/10.1113/JP270604.